Direct numerical simulation of streamwise traveling wave induced turbulent pipe flow relaminarization

Journal of Physics: Conference Series **3173** (2026) 012003 doi:10.1088/1742-6596/3173/1/012003

Direct numerical simulation of streamwise traveling wave induced turbulent pipe flow relaminarization

Christian Bauer[1] **and Claus Wagner**[1,2]

[1]Institute of Aerodynamics and Flow Technology, German Aerospace Center Göttingen, Germany

[2]Institute of Thermodynamics and Fluid Mechanics, Technische Universität Ilmenau, Germany

E-mail: christian.bauer@dlr.de

Abstract. In pipe flows at high Reynolds numbers, more than 90% of the pumping power is dissipated by near-wall turbulence, making relaminarization a promising strategy for saving energy. Streamwise traveling waves of wall blowing and suction, previously proven able to relaminarize turbulent pipe flow at $\mathrm{Re}\tau = u_\tau R/\nu = 110$, are here demonstrated to achieve relaminarization up to $\mathrm{Re}\tau = 540$. Here, u_τ is the friction velocity, R the pipe radius, and ν the kinematic viscosity. Independent of the Reynolds number, the relaminarization requires $130R/u_\tau$ for the drag reduction rate to converge. The resulting flow structure combines viscous-scaled half-vortices superimposed on the radius-scaled laminar profile. These results establish scaling relations that extend traveling wave–induced relaminarization to higher Reynolds numbers, offering a predictive framework for energy-efficient flow control.

1 Introduction

For technically relevant flows with high Reynolds numbers, more than 90% of the energy required to pump fluids through pipes is dissipated by turbulence near the wall. Therefore, flow control methods often aim at minimizing or laminarizing wall turbulence.

Min et al. [1] employed a direct numerical simulation (DNS) of turbulent plane channel flow with upstream traveling waves (UTWs) of blowing and suction at a bulk Reynolds number of $Re_b = u_b D/\nu = 2000$, where u_b is the bulk velocity, D is the pipe diameter, and ν is the kinematic viscosity. They showed that UTWs induce a negative Reynolds shear stress, causing a skin friction drag reduction below that of the corresponding laminar flow. For a channel flow without a mean pressure gradient, Hoepffner and Fukagata [2] presented that traveling waves of wall blowing and suction induce a bulk flow in the opposite direction of the traveling waves—a mechanism that is denoted as the pumping effect. Although UTWs can cause sublaminar drag due to the pumping effect, the total energy needed to drive and control the main flow can not be lower than the energy needed to drive the corresponding laminar flow [3, 4]. While UTWs destabilize the flow, Moarref and Jovanovich [5] predicted that the onset of turbulence in channel flow can be controlled by downstream traveling waves (DTWs) with specific speed and frequency. Lieu et al. [6] confirmed these predictions utilizing a low Reynolds number DNSs at $\mathrm{Re}_\tau = u_\tau h/\nu = 63$. They illustrated that DTWs can relaminarize fully-developed turbulent channel flow, whereas UTWs induce turbulence to a laminar base flow. Mamori et al. [7] performed a parametric study at $\mathrm{Re}_\tau = 110$ and $\mathrm{Re}_\tau = 300$ varying the amplitude a, wavelength λ, and celerity c of the traveling waves. For DTWs, they determined the effective parameter range for relaminarization, i.e. $a > 0.1U_{b,lam}$, $c > 1.5U_{b,lam}$,

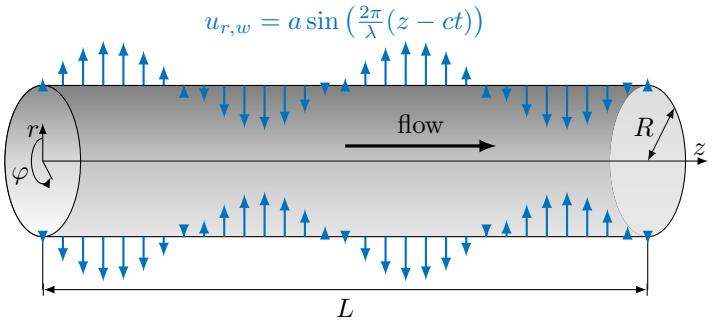

Figure 1: Pipe geometry with a cylindrical coordinate system, where z is the axial, φ the azimuthal and r the radial coordinate. L is the pipe length and R the pipe radius. At the pipe wall the wall-normal velocity is set to $u_{r,w} = a\sin(2\pi/\lambda(z - ct))$.

and $200 < \lambda^+ < 500$, where $U_{b,lam}$ is the bulk velocity of the corresponding laminar flow. Additionally, Mamori et al. [7] achieved a drag reduction rate of 0.15 with UTWs for $\mathrm{Re}_\tau = 110$.

With respect to turbulent pipe flow, Koganezawa et al. [8] verified for the low friction Reynolds number of $\mathrm{Re}_\tau = u_\tau R/\nu = 110$—$R$ being the pipe radius—that with similar wave parameters as for channel flow [7], downstream traveling waves of wall blowing/suction can lead to relaminarization. In addition, Fukagata et al. [9] noted that higher Reynolds number data are essential for engineering applications. Consequently, Bauer and Wagner [10] explored the scaling of the wave parameters required for significant energy savings related to the relaminarization of the flow. In agreement with both earlier pipe flow studies [8] and channel flow studies [7], Bauer and Wagner [10] verified that traveling wave amplitude a and speed c that lead to the maximal net energy savings scale with the centerline velocity of the corresponding laminar flow $U_{c,lam}$, whereas the wavelength λ scales with the viscous length scale $\delta_\nu = \nu/u_\tau$. In the present study, we are going to examine the DTW-induced turbulent pipe flow relaminarizaion at $180 \leq \mathrm{Re}_\tau \leq 540$, utilizing the data we published in Bauer and Wagner [10].

2 Numerical methodology

We are solving the incompressible Navier-Stokes equations for a Newtonian fluid in a smooth pipe, i.e.

$$\frac{\partial \vec{u}}{\partial t} + \vec{u}\cdot\nabla\vec{u} + \nabla p = \frac{1}{\mathrm{Re}_\tau}\nabla^2\vec{u}, \tag{1}$$

$$\nabla\cdot\vec{u} = 0, \tag{2}$$

with the friction Reynolds number $\mathrm{Re}_\tau = u_\tau R/\nu$, where R is the pipe radius. After being spatially discretized using a fourth-order finite volume method, equation (2) is integrated in time based on a leapfrog-Euler time integration scheme [11, 12, 13]. Figure 1 presents the flow geometry, which is a smooth pipe with length L and radius R. At the wall, the no-slip boundary condition is applied to the axial and azimuthal velocity component, i.e. $u_{z,w} = u_{\varphi,w} = 0$, whereas the wall-normal velocity component is set to a traveling-wave-like velocity profile,

$$u_{r,w} = u_r(z, \varphi, r = R) = a\sin\left(\frac{2\pi}{\lambda}(z - ct)\right), \tag{3}$$

where a is the wave amplitude, λ the wavelength, and c the wave speed. Based on the parameters Re_τ, a, λ, and c a set of DNSs has been performed [10]. Bauer and Wagner [10] pointed out that for certain wave parameters, DTWs relaminarize the flow independent of the Reynolds number, while saving remarkable amounts of energy. Table 1 presents selected cases of DTW-induced flow relaminarization for friction Reynolds numbers of $180 \leq \mathrm{Re}_\tau \leq 540$.

3 Results

For the present simulations under constant pressure gradient, a reduction of drag manifests in an increase of bulk velocity. Hence, the friction drag coefficient is computed as

$$C_f = \frac{2\tau_w}{\rho u_b^2} = \frac{2}{u_b^{+2}}, \tag{4}$$

Table 1: Selected flow cases: Re_τ = is the friction Reynolds number, a^+, λ^+, and c^+ are the amplitude, the wavelength, and the celerity of the traveling wave boundary condition in wall units. N_z, N_ϕ, and N_r are the number of grid points with respect to the axial, azimuthal, and radial direction, respectively. Δz^+, streamwise grid spacing; $R^+\Delta\varphi$ azimuthal grid spacing at the wall; Δr^+_{min}, minimal radial grid spacing.

case	Re_τ	a^+	λ^+	c^+	N_z	N_φ	N_r	Δz^+	$R^+\Delta\varphi$	Δr^+	line
1	180	6	360	90	768	256	84	4.7	4.4	0.31	
2	360	13.5	360	180	1024	512	160	4.9	4.4	0.39	
3	540	24.0	360	270	1536	1024	222	4.9	3.3	0.37	

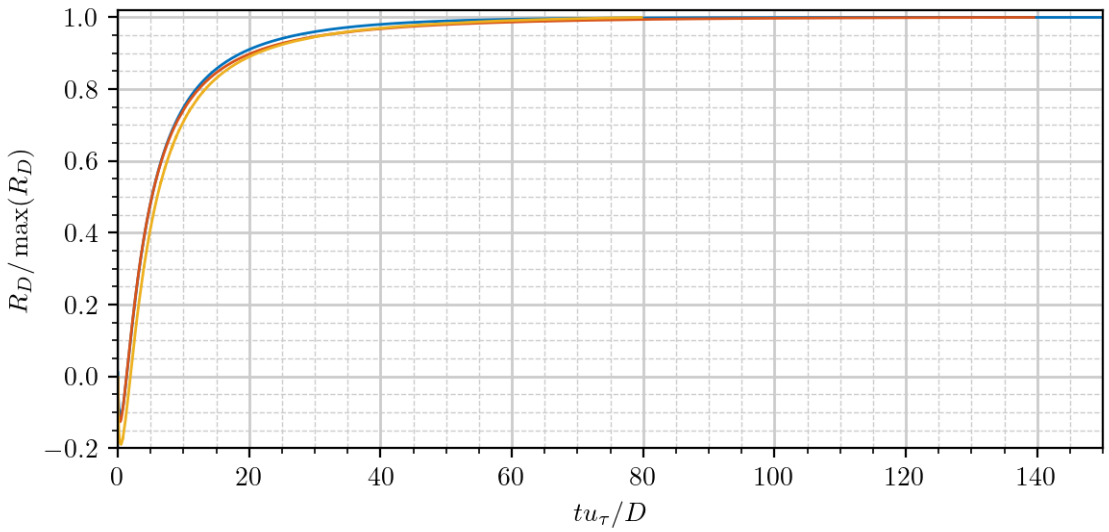

Figure 2: Time series of the drag reduction rate R_D normalized by its maximum for relaminarization cases at $\mathrm{Re}_\tau = 180$ (blue line), $\mathrm{Re}_\tau = 360$ (red line), and $\mathrm{Re}_\tau = 540$ (yellow line); see Table1.

with the wall shear stress τ_w, the fluid density ρ, and the bulkd velocity u_b. The superscript + denotes normalization in wall units, i.e. normalization with the friction velocity u_τ for velocities and the viscous length scale $\delta_\nu = \nu/u_\tau$, with the kinematic viscosity ν, for length scales. The drag reduction rate is then computed as follows:

$$R_D = \frac{C_{f0} - C_f}{C_{f0}}, \tag{5}$$

where C_{f0} is the skin friction coefficient of the uncontrolled case either at the same friction Reynolds number or at the same bulk Reynolds number as the uncontrolled flow. In case of relaminarization, the drag reduction rate settles after and initial transient of approximately $65D/u_\tau$ [10]. Moreover, Bauer and Wagner [10] reported that the converged drag reduction rate increases with the friction Reynolds number, i.e. $0.82 \leq R_D \leq 0.95$ for $180 \leq \mathrm{Re}_\tau \leq 540$. Figure 2 features the drag reduction rate R_D normalized by its maximum $\max(R_D)$ for the relaminarization cases depicted in Table 1. Figure 2 shows the collapse of the drag reduction rate time series normalized by their respective maximums for the different Reynolds numbers. Therefore, the acceleration of the flow to its terminal velocity is independent of the Reynolds number. Specifically, 99% of the maximum drag reduction rate is reached after approximately $65D/u_\tau$.

Figure 3 illustrates instantaneous flow field realizations at $t = 0.01D/u_\tau$ (left), $t = 0.8D/u_\tau$ (middle), and $t = 114.3D/u_\tau$ (right) for case 1 at $\mathrm{Re}_\tau = 180$. When the flow relaminarizes, the streamwise velocity component u_z accelerates significantly (Figure 3a,b,c). Conversely, the azimuthal velocity component u_φ decays to zero, as seen in Figure 3(d,e,f). Besides, during relaminarization, the turbulent fluctuations visible at the beginning of the control period in Figure 3(g) are removed from the radial velocity component u_r, and only the periodic component engendered by the traveling wave control input remains

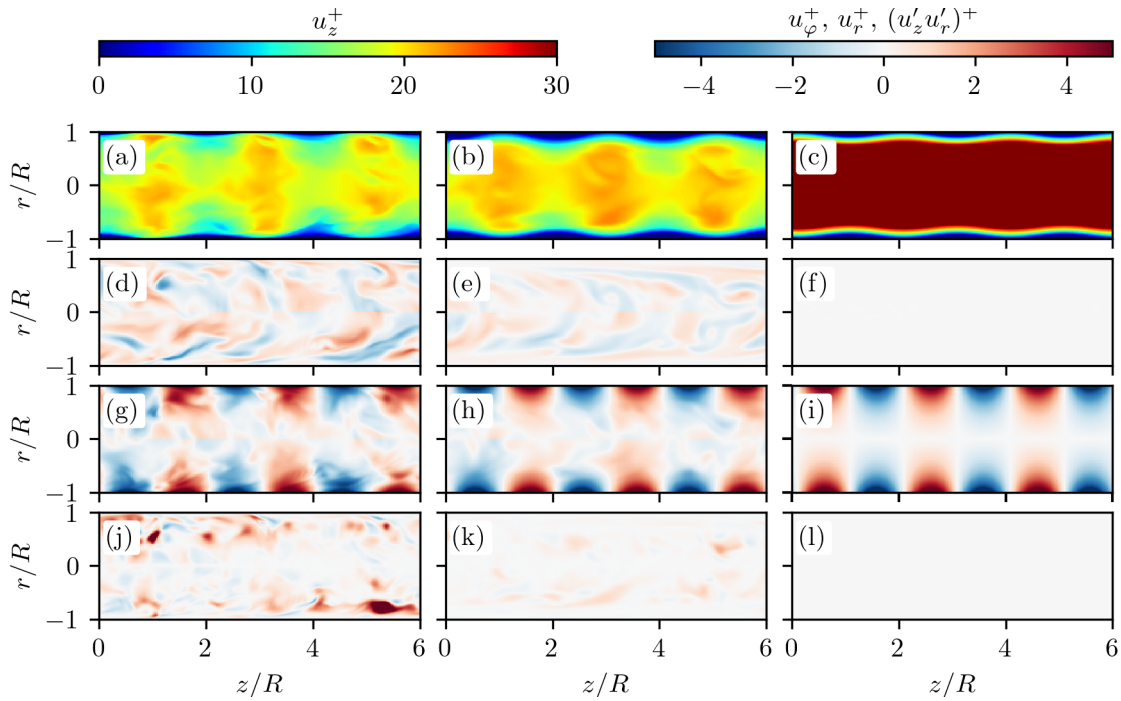

Figure 3: Instantaneous flow field realization of case 1 ($a^+ = 6$, $\lambda^+ = 360$, $c^+ = 90$) at $tu_\tau/D = 0.01$ (a,d,g,j), $tu_\tau/D = 0.8$ (b,e,h,k), and $tu_\tau/D = 114.3$ (c,f,i,l) after the start of the control. Velocity components u_z^+ (a,b,c) u_φ^+ (d,e,f), and u_r^+ (g,h,i). Instantaneous Reynolds shear stress $(u_z'u_r')^+$ (j,k,l).

(Figure 3i). Moreover, the decrease of the turbulent velocity fluctuations causes the turbulent Reynolds shear stress, depicted in Figure 3(j,k,l), to decay to zero, thereby lowering drag. As illustrated in Figure 4 and Figure 5, similar observations emerge from the instantaneous flow field realizations corresponding to case 2 ($\mathrm{Re}_\tau = 360$) and case 3 ($\mathrm{Re}_\tau = 540$), respectively. As the friction Reynolds number increases from $\mathrm{Re}_\tau = 180$ (Figure 3) to $\mathrm{Re}_\tau = 360$ (Figure 4) and then to $\mathrm{Re}_\tau = 540$ (Figure 5), the range of turbulent scales expands, with the small structures scaling in viscous units. Consequently, the small scale turbulent structures observed at the start of the controlled period ($t = 0.01D/u_\tau$) across the three velocity components, as well as the turbulent Reynolds shear stress, decrease in size as $\mathrm{Re}_\tau = 180$ increases. This trend is evident when comparing Figure 3(a,d,g,j) to Figure 4(a,d,g,j) and Figure 5(a,d,g,j). Additionally, the periodic flow structures triggered by the traveling wave, most pronounced in the radial velocity component u_r after the flow has been relaminarized in Figure 3(i), Figure 3 4(i), and Figure 3 5(i), scale in viscous units (see also Bauer and Wagner [10]).

After the flow has reached a statistically-stationary state, phase-averaged statistics are computed as follows:

$$\langle\phi\rangle_{N_{\phi_z}\varphi t}(\tilde{z},r) = \frac{1}{2\pi T N_{\phi_z}} \sum_{z\in N_{\phi_z}} \left(\int_{t_0}^{t_0+T} \int_0^{2\pi} \phi(z,\varphi,r,t) d\varphi dt \right), \tag{6}$$

with $N_{\phi_z} = L/\lambda$ the number of streamwise locations of the same phase and $\tilde{z} = \lambda n + (z - ct)$ the streamwise coordinate in phase space, with the integer n and $0 \leq \tilde{z} \leq \lambda$ streamwise and radial velocity components. In addition, we implement the triple decomposition introduced by Hussain and Reynolds [14],

$$\phi(z,\varphi,r,t) = \langle\phi\rangle_{z\varphi t}(r) + \tilde{\phi}(\tilde{z},r) + \phi''(z,\varphi,r,t), \tag{7}$$

with the spatio-temporal average,

$$\langle\phi\rangle_{z\varphi t}(r) = \frac{1}{2\pi L T} \int_{t_0}^{t_0+T} \int_0^L \int_0^{2\pi} \phi(z,\varphi,r,t) d\varphi dz dt, \tag{8}$$

the periodic component,

$$\tilde{\phi}(\tilde{z},r) = \langle\phi\rangle_{N_{\phi_z}\varphi t}(\tilde{z},r) - \langle\phi\rangle_{z\varphi t}(r), \tag{9}$$

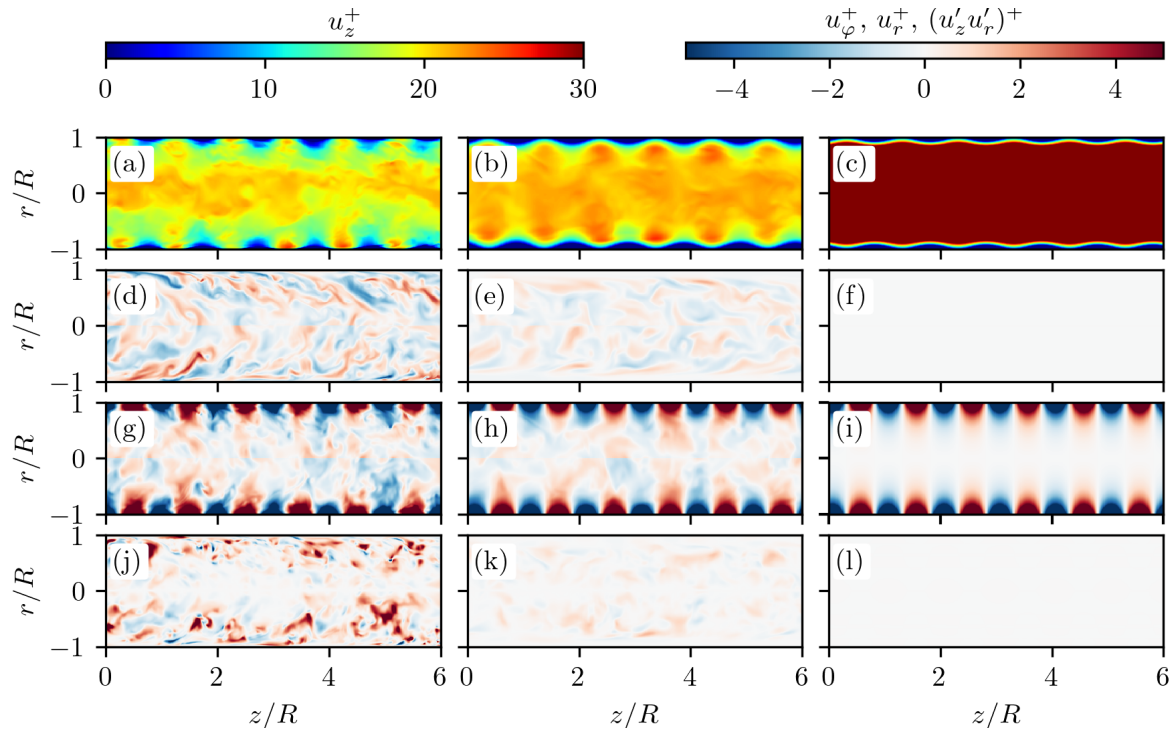

Figure 4: Instantaneous flow field realization of case 2 ($a^+ = 13.5$, $\lambda^+ = 360$, $c^+ = 180$) at $tu_\tau/D = 0.01$ (a,d,g,j), $tu_\tau/D = 0.8$ (b,e,h,k), and $tu_\tau/D = 143.5$ (c,f,i,l) after the start of the control. Velocity components u_z^+ (a,b,c) u_φ^+ (d,e,f), and u_r^+ (g,h,i). Instantaneous Reynolds shear stress $(u_z'u_r')^+$ (j,k,l).

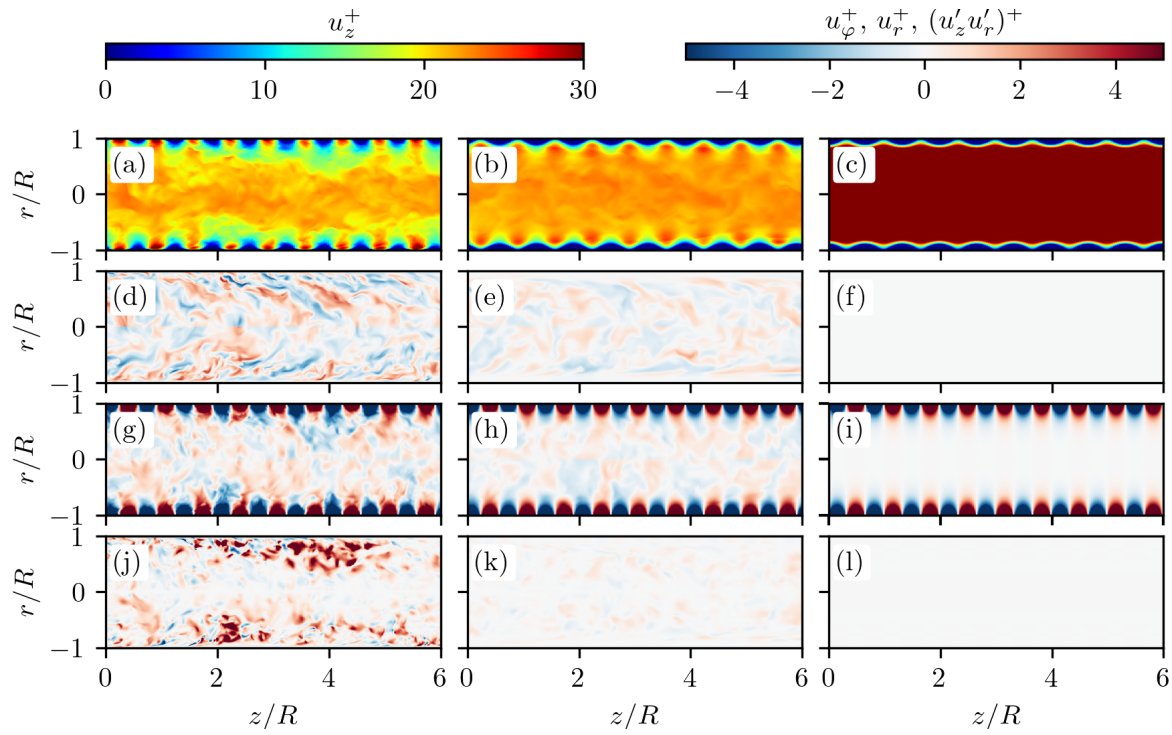

Figure 5: Instantaneous flow field realization of case 3 ($a^+ = 24$, $\lambda^+ = 360$, $c^+ = 270$) at $tu_\tau/D = 0.01$ (a,d,g,j), $tu_\tau/D = 0.8$ (b,e,h,k), and $tu_\tau/D = 54.8$ (c,f,i,l) after the start of the control. Velocity components u_z^+ (a,b,c) u_φ^+ (d,e,f), and u_r^+ (g,h,i). Instantaneous Reynolds shear stress $(u_z'u_r')^+$ (j,k,l).

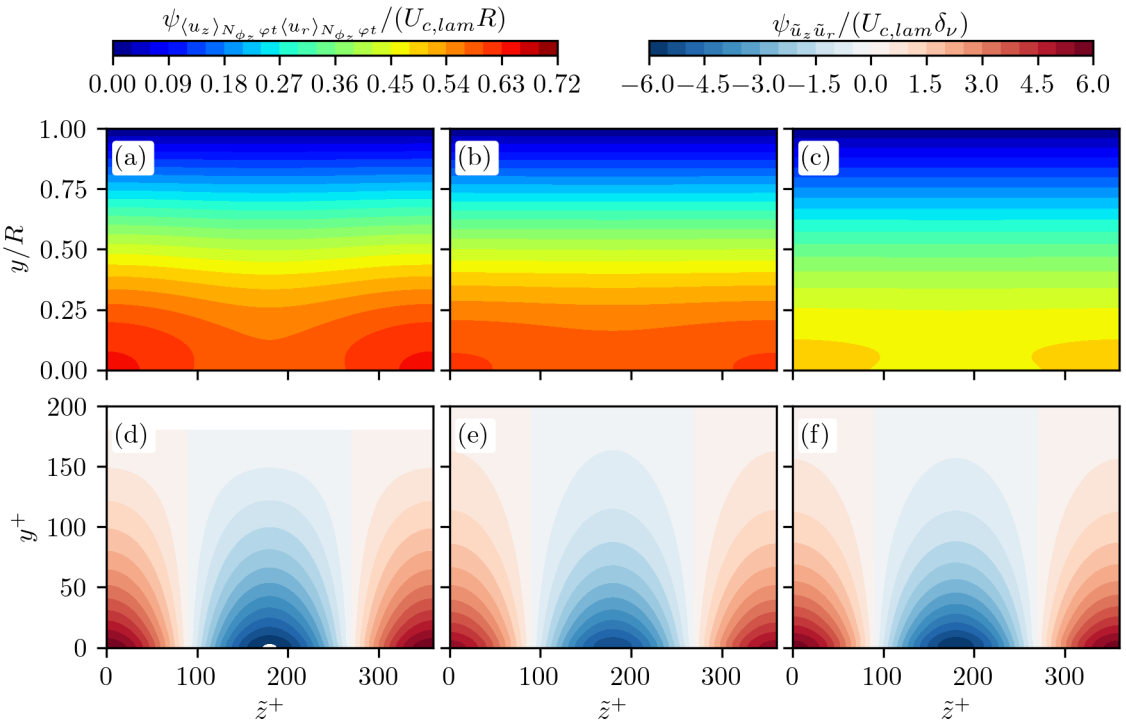

Figure 6: Stream function of the phase-averaged streamwise and radial velocity normalized by $U_{c,lam}$ and R (a,b,c) and stream function of the periodic component of the streamwise and radial velocity normalized by $U_{c,lam}$ and δ_ν (d,e,f) for case 1 (a,d), case 2 (b,e), and case 3 (c,f).

as well as the turbulent component $\phi''(z,\varphi,r,t)$. From the phase-averaged velocity components, we compute the streamfunction $\psi_{\langle u_z\rangle_{N_{\phi_z}\varphi t}\langle u_r\rangle_{N_{\phi_z}\varphi t}}$ that satisfies the condition

$$\begin{pmatrix}\partial\psi_{\langle u_z\rangle_{N_{\phi_z}\varphi t}\langle u_r\rangle_{N_{\phi_z}\varphi t}}/\partial z\\ \partial\psi_{\langle u_z\rangle_{N_{\phi_z}\varphi t}\langle u_r\rangle_{N_{\phi_z}\varphi t}}/\partial r\end{pmatrix}=\begin{pmatrix}-\langle u_r\rangle_{N_{\phi_z}\varphi t}\\ \langle u_z\rangle_{N_{\phi_z}\varphi t}\end{pmatrix}. \tag{10}$$

Figure 6 displays iso-contours of the phase-averaged velocity's streamfunction $\psi_{\langle u_z\rangle_{N_{\phi_z}\varphi t}\langle u_r\rangle_{N_{\phi_z}\varphi t}}$ (a,b,c) normalized with the corresponding laminar flow centerline velocity $U_{c,lam} = 1/2\mathrm{Re}_\tau u_\tau$ and the pipe radius R, as well as iso-contours of the periodic velocity component's streamfunction $\psi_{\tilde{u}_z\tilde{u}_r}$ (d,e,f) normalized with $U_{c,lam}$ and the viscous length scale δ_ν. Figure 6(a,b,c) lays out that the streamfunction appears to scale with $U_{c,lam}$ and R away from the wall, whereas near the wall coherent structures are visible that are not scaling with the pipe radius. These structures, which are generated by the DTW boundary condition, are revealed by the streamfunction of the periodic velocity component depicted in Figure 6(d,e,f). Figure 6(d,e,f) shows counter-rotating half vortices which periodically accelerate and decelerate the flow. These elliptical vortices scale in wall units, with a minor diameter of $d_z^+ = \frac{1}{2}\lambda^+ = 180$ and a major diameter of $d_y^+ \approx 300$.

4 Conclusion

Using DNSs, we demonstrated that DTWs relaminarize initially turbulent pipe flow at friction Reynolds numbers of $180 \leq \mathrm{Re}_\tau \leq 540$. While turbulent fluctuation decay rapidly after the onset of the control period, the acceleration of the flow takes much longer. Consequently, the drag reduction rate R_D varies less than 1% of its terminal value after approximately $65D/u_\tau$. The ensuing flow structure combines viscous-scaled half-vortices super-imposed on the radius-scaled laminar profile. These results establish scaling relations that extend traveling wave–induced relaminarization to higher Reynolds numbers, offering a predictive framework for energy-efficient flow control.

Acknowledgements
The authors sincerely appreciate the careful and conscientious proofreading provided by Mahsa Pakzad. The authors gratefully acknowledge the scientific support and HPC resources provided by the German Aerospace Center (DLR). The HPC system CARO is partially funded by "Ministry of Science and Culture of Lower Saxony" and "Federal Ministry for Economic Affairs and Climate Action".

References

[1] Taegee Min, Sung Moon Kang, Jason L. Speyer, and John Kim. Sustained sub-laminar drag in a fully developed channel flow. *Journal of Fluid Mechanics*, 558:309, 2006.

[2] Jérôme Hœpffner and Koji Fukagata. Pumping or drag reduction? *Journal of Fluid Mechanics*, 635:171–187, 2009.

[3] Thomas R. Bewley. A fundamental limit on the balance of power in a transpiration-controlled channel flow. *Journal of Fluid Mechanics*, 632:443–446, 2009.

[4] Koji Fukagata, Kazuyasu Sugiyama, and Nobuhide Kasagi. On the lower bound of net driving power in controlled duct flows. *Physica D: Nonlinear Phenomena*, 238(13):1082–1086, 2009.

[5] Rashad Moarref and Mihailo R. Jovanović. Controlling the onset of turbulence by streamwise travelling waves. Part 1. Receptivity analysis. *Journal of Fluid Mechanics*, 663:70–99, 2010.

[6] Binh K. Lieu, Rashad Moarref, and Mihailo R. Jovanović. Controlling the onset of turbulence by streamwise travelling waves. Part 2. Direct numerical simulation. *Journal of Fluid Mechanics*, 663:100–119, 2010.

[7] H. Mamori, K. Iwamoto, and A. Murata. Effect of the parameters of traveling waves created by blowing and suction on the relaminarization phenomena in fully developed turbulent channel flow. *Physics of Fluids*, 26(1):015101, 2014.

[8] S. Koganezawa, A. Mitsuishi, T. Shimura, K. Iwamoto, H. Mamori, and A. Murata. Pathline analysis of traveling wavy blowing and suction control in turbulent pipe flow for drag reduction. *International Journal of Heat and Fluid Flow*, 77:388–401, 2019.

[9] Koji Fukagata, Kaoru Iwamoto, and Yosuke Hasegawa. Turbulent Drag Reduction by Streamwise Traveling Waves of Wall-Normal Forcing. *Annual Review of Fluid Mechanics*, 56(1):69–90, 2024.

[10] Christian Bauer and Claus Wagner. Relaminarization of turbulent pipe flow induced by streamwise traveling wave wall transpiration and its scaling. *Acta Mechanica (submitted)*, 2026.

[11] Daniel Feldmann and Claus Wagner. Test Direct numerical simulation of fully developed turbulent and oscillatory pipe flows at $\mathrm{Re}_\tau = 1440$. *Journal of Turbulence*, 13(32):1–28, 2012.

[12] Daniel Feldmann, Christian Bauer, and Claus Wagner. Computational domain length and Reynolds number effects on large-scale coherent motions in turbulent pipe flow. *Journal of Turbulence*, 19(3):274–295, 2018.

[13] Christian Bauer, Daniel Feldmann, and Claus Wagner. On the convergence and scaling of high-order statistical moments in turbulent pipe flow using direct numerical simulations. *Physics of Fluids*, 29(12):125105, 2017.

[14] A. K. M. F. Hussain and W. C. Reynolds. The mechanics of an organized wave in turbulent shear flow. *Journal of Fluid Mechanics*, 41(2):241–258, 1970.